

Article

Influence of Deposition Conditions and Thermal Treatments on Morphological and Chemical Characteristics of $\text{Li}_{6.75}\text{La}_3\text{Zr}_{1.75}\text{Ta}_{0.25}\text{O}_{12}$ Thin Films Deposited by Nanosecond PLD

Mariangela Curcio ^{1,*} , Sergio Brutti ^{2,3} , Arcangelo Celeste ² , Agostino Galasso ¹, Angela De Bonis ^{1,3,*}  and Roberto Teghil ¹ 

¹ Dipartimento di Scienze, Università della Basilicata, Viale dell'Ateneo Lucano 10, 85100 Potenza, Italy; agostino.galasso@unibas.it (A.G.); roberto.teghil@unibas.it (R.T.)

² Dipartimento di Chimica, Università di Roma La Sapienza, Piazzale Aldo Moro 5, 00185 Roma, Italy; sergio.brutti@uniroma1.it (S.B.); arcangelo.celeste@uniroma1.it (A.C.)

³ GISEL-Centro di Riferimento Nazionale per i Sistemi di Accumulo Elettrochimico di Energia, INSTM via G. Giusti 9, 50121 Firenze, Italy

* Correspondence: mariangela.curcio@unibas.it (M.C.); angela.debonis@unibas.it (A.D.B.)

Abstract: The production of thin films has been extensively studied due to their unique properties that make them highly useful in a wide range of scientific and technological applications. Obtaining thin films with well-defined stoichiometry and crystallinity is a challenging task, especially when dealing with materials of complex stoichiometry. Among diverse methodologies for the manufacture of thin films, pulsed laser deposition (PLD) stands out as a versatile technique for producing crystalline films with complex chemical compositions. In this study, nanosecond PLD was employed to manufacture thin films of Ta-doped $\text{Li}_7\text{La}_3\text{Zr}_2\text{O}_{12}$ (LLZTO), a garnet-like oxide that has been proposed as solid electrolyte for Li-ion solid state batteries. Two distinct deposition atmospheres were investigated: vacuum conditions at 10^{-3} Pa and an oxygen-enriched environment with 10 Pa of O_2 gas buffer. To mitigate lithium losses during deposition, a minor addition of lithium oxide was incorporated into the target. The effects of deposition atmosphere and the impact of post-deposition annealing on the structural, compositional, and morphological properties of LLZTO thin films were analysed through a multi-technique approach. The results suggest deposition under oxygen pressure led to the growth of compact, crystalline films characterized by homogenous elemental distribution across the surface and throughout the film's depth. These films closely resemble the composition of the target LLZTO material, offering valuable insights for the fabrication of high-quality complex oxide thin films.

Keywords: pulsed laser deposition; complex material; influence of gas buffer; thin films; solid-state electrolytes; Ta-doped LLZO



Citation: Curcio, M.; Brutti, S.; Celeste, A.; Galasso, A.; De Bonis, A.; Teghil, R. Influence of Deposition Conditions and Thermal Treatments on Morphological and Chemical Characteristics of $\text{Li}_{6.75}\text{La}_3\text{Zr}_{1.75}\text{Ta}_{0.25}\text{O}_{12}$ Thin Films Deposited by Nanosecond PLD. *Coatings* **2023**, *13*, 1496. <https://doi.org/10.3390/coatings13091496>

Academic Editor: Alberto Palmero

Received: 7 August 2023

Revised: 22 August 2023

Accepted: 23 August 2023

Published: 24 August 2023



Copyright: © 2023 by the authors. Licensee MDPI, Basel, Switzerland. This article is an open access article distributed under the terms and conditions of the Creative Commons Attribution (CC BY) license (<https://creativecommons.org/licenses/by/4.0/>).

1. Introduction

Thin films have proven to be crucial in driving advancements across various scientific and technological fields, including electronics, photonics, energy storage, catalysis, and sensing. The possibility to modify and enhance the properties of bulk materials when converted in thin films form has opened new opportunity for innovation and progress.

Among the various techniques for film deposition, pulsed laser deposition (PLD) offers significant advantages including the possibility to preserve the target composition and stoichiometry. It is a well-known technique that involves the use of a pulsed laser beam to ablate material from a solid target and deposit it onto a substrate, forming a thin film. The interaction between a pulsed laser beam and the target material causes the absorption of the laser photons. By using a laser source in the nanosecond time regime, the absorption of the laser pulse is followed by a thermal diffusion process, which leads to vaporization

and plasma formation during the pulse time [1]. The laser induced plasma is composed of atoms, molecules, ions, electrons and clusters and its composition and expansion are strongly correlated to deposition parameters, first and foremost the ambient background (i.e., vacuum, background inert or reactive gas) and the laser parameters (pulse duration, wavelength and fluence).

PLD allows deposition within a broad pressure range, spanning from ultra-high vacuum to ambient pressure [2]. Moreover, this technique enables the deposition of the widest range of accessible material compositions and stands as the most efficient method for materials with complex chemical compositions [2,3]. However, it requires careful optimization of the experimental parameters to achieve high-quality crystalline films with the desired composition. During the laser ablation of a target material composed by atoms with relevant mass differences, the lighter elements are more accelerated than the heavier ones and scattered towards the peripheral region of the plasma. This process depletes the plasma from lighter elements in the target-to-substrate direction with respect to the heavier ones. Therefore, despite their larger velocity, the relative concentration of lighter elements in the deposited film is smaller compared to the heavier ones due to scattering [2–4]. This phenomenon unavoidably contributes to considerable compositional deviation: this is true for solid state lithium ionic conductors like $\text{Li}_7\text{La}_3\text{Zr}_2\text{O}_{12}$ (LLZO) where very light atoms, e.g., Li, and very heavy ones, e.g., Zr and La, coexist.

The use of solid electrolytes offers several advantages in lithium and sodium batteries compared to traditional liquid electrolytes. One of the most significant advantages is their improved safety profile with respect to liquid electrolytes, with reduced risk of fires and explosions. Polymeric [5] and inorganic [6] electrolytes have been proposed. Among inorganic electrolytes LLZO garnet presents high Li^+ conductivity and high electrochemical stability against Li. LLZO can crystallize in two polymorphs: the tetragonal phase (t-LLZO) that is stable at low temperature and the cubic phase (c-LLZO) that is stable above 250–750 °C. The c-LLZO is characterized by an ionic conductivity two orders of magnitude larger than t-LLZO but is unfortunately unstable at room temperature. In order to stabilize the cubic phase at room temperature, doping has been demonstrated to play a pivotal role: as an example isovalent cations can substitute Zr in the lattice (e.g., Ta or Nb), and/or aliovalent cations can substitute Li atoms (e.g., Al or Ga) [7,8]. Among the multiple available doping strategies already demonstrated in the literature, tantalum-doping of LLZO has proven to be one of the most favorable exhibiting higher ion conductivity and stability with respect to many others. [9,10]. In addition, Ta-doped LLZO thin films have been already demonstrated to disclose remarkable improvement in the lithium-ion conductivity compared to bulks, thanks (a) to the reduction of the diffusion thickness to nanoscale dimensions and (b) to the minimization of 0D-1D defects and grain boundaries [11]. On the other hand, the instability of LLZO in ambient air with the formation of LiOH and Li_2CO_3 strongly impairs its ionic conductivity the surface of LLZO particles. It has recently showed that the rate constants of hydration and carbonation kinetics for LLZO linearly depend from the surface area of particles size [12]. Mechanical, thermal and chemical removal of contaminants have been proposed, but it was recently reported that it is possible to improve the air stability of LLZO controlling of the processing atmosphere [13] and tailoring the grain boundaries with aliovalent elements [14].

In solid state microbatteries, positive and negative electrodes are separated by a thin film of a solid state electrolyte. Several approaches were developed to deposit thin films of electrolyte retaining the pristine stoichiometry and crystal structure also minimizing the grain boundaries [6]. PLD has been successfully employed for the deposition of thin films of cathode, anode and solid electrolyte materials [15,16].

In this study PLD has been exploited to manufacture thin films of LLZTO (i.e., Ta-doped LLZO: $\text{Li}_{6.75}\text{La}_3\text{Zr}_{1.75}\text{Ta}_{0.25}\text{O}_{12}$) [7]. A nanosecond-pulsed laser source (i.e., second harmonic of Nd:YAG laser) has been employed and the influence of deposition atmosphere on the PLD film manufacture has been investigated by depositing in vacuum (10^{-3} Pa) and at 10 Pa of O_2 static gas pressure. Moreover, with the aim to improve film crystallinity,

post-deposition thermal processing at 600 °C in air and in O₂ has been carried out [17–19]. Additionally, Li₂O (6 wt%) was added to the target material to compensate the Li-losses during the PLD. The physicochemical characterization of the thin films has been carried out by a multi-technique approach that includes micro-Raman, XRD, SEM, and TEM.

2. Materials and Methods

The PLD of LLZTO was performed inside a stainless steel vacuum chamber using a frequency-doubled Nd:YAG laser source (Handy YAG Quanta System Q-switched) (Quanta System, Milano, Italia), with $\lambda = 532$ nm, $\tau = 10$ ns, and repetition rate = 10 Hz. The depositions were conducted at $30 \text{ J} \times \text{cm}^{-2}$ of fluence, for a deposition time of 3 h, with a target-substrate distance of 2 cm, at room temperature. S316 steel foils (SS foil, MTI Corporation, Richmond, VA, USA) were cut in round discs with a diameter of 2 cm and used as substrates. The target material was obtained by pressing commercial powders (MTI Corp) (MTI Corporation, Richmond, VA, USA) into pellets and placed on a rotating holder to avoid piercing during the ablation. Two target composition have been considered: LLZTO and LLZTO enriched with 6 wt% of Li₂O (Sigma-Aldrich, St. Louis, MO, USA) (LLZTO + Li₂O). Different sets of samples were produced, as summarized in the Table 1. For the deposition in O₂ atmosphere, the chamber was previously evacuated at $\sim 10^{-3}$ Pa, then it was filled with gas and the pressure was kept at around 10 Pa during the deposition. Film thickness was of about 700 and 500 nm for films deposited at 10^{-3} Pa and 10 Pa of O₂, respectively.

Table 1. Sample manufacture experimental conditions.

Target Material	Deposition Pressure	Annealing Condition
LLZTO	10^{-3} Pa	none
	10 Pa O ₂	
LLZTO + Li ₂ O	10^{-3} Pa	none
	10 Pa O ₂	
LLZTO + Li ₂ O	10^{-3} Pa	In air, heating $10 \text{ }^\circ\text{C min}^{-1}$, rest at $600 \text{ }^\circ\text{C}$ for 5 min, natural cooling
	10 Pa O ₂	
LLZTO + Li ₂ O	10^{-3} Pa	Under O ₂ flow (80 mL min^{-1}), heating $10 \text{ }^\circ\text{C min}^{-1}$, rest at $600 \text{ }^\circ\text{C}$ for 5 min, natural cooling
	10 Pa O ₂	

Transmission electron microscopy (TEM—FEI TECNAI, G2 20 TWIN, operating at 200 kV) analysis was carried out on samples deposited for 10 min on FORMAR-Carbon copper grids (Agar Scientific, Stansted, UK) A Philips FEI ESEM XL30 scanning electron microscope (FEI, Hillsboro, OR, USA), equipped with an Energy Dispersive X-ray Spectroscopy (EDX) apparatus, was utilized. FIB-SEM (Focus Ion Beam Scanning Electron Microscopy)-HR FESEM Zeiss Auriga apparatus (ZEISS, Jena, Germany) was used for cross sectional analysis of films with a FIB-milling resolution of 2.5 nm. The films crystal structure was verified through X-ray diffraction (XRD) (Siemens, Munich, Germany) measurements performed with a Siemens D5000 diffractometer in the following conditions: CuK α radiation ($\lambda = 1.5405600 \text{ \AA}$), $2\theta = 15^\circ\text{--}60^\circ$, step size 0.040° , time per step 4 s. For micro-Raman spectroscopy a HORIBA LabRAM HR 800 apparatus (Horiba, Ltd., Kyoto, Japan), equipped with edge filter, which excludes Raman shift below 150 cm^{-1} from detection, and a He–Ne laser ($\lambda = 632.8 \text{ nm}$), coupled with an Olympus microscope, was employed. All the spectra were acquired with a 600 gr mm^{-1} grating, in the range $200\text{--}1000 \text{ cm}^{-1}$, with an accumulation time of 60 s.

3. Results and Discussion

3.1. PLD Films from Stoichiometric LLZTO Targets

Among the many PLD manufacturing parameters, the control of the deposition atmosphere can promote specific film morphologies, surface chemistries or moieties thus allowing a fine tailoring of the film characteristics for specific applications. For PLD experiments, the ambient pressure has strong impact on the condensation rate from the plasma, film growth rate, and film quality, because it affects the plasma plume expansion, composition and transport of the ablated species to the substrate. PLD depositions carried out under high pressures leads to compact and dense films whereas lower pressures can promote the film adhesion over the substrate or reduce impurity incorporation [3]. Furthermore, the background gas plays an important role in the film growth and properties, since it helps to create a controlled environment, shielding the ablated material from reactive species or contaminants during the deposition, like the inevitable water moisture or hydrocarbons, leading to high purity films with improved properties.

With regard to the deposition pressure, one can refer to the classification made by Amoruso et al. [20] for the deposition atmosphere. In particular, three different regimes based on the pressure of the deposition chamber have been defined: (a) “vacuum” ($\leq 10^{-1}$ Pa), in which no interactions between gas buffer and plasma occur; (b) “transition” (10^{-1} –1 Pa) in which such interactions start to take place, and, at higher pressure, the “diffusion-like” regime, characterized by a plasma with a slower expansion and a broad angular distribution [21]. In vacuum regime ablated species inside the plasma are characterized by high but varied velocities: as a consequence, the various atomic or cluster species impact on the substrate surface with different time delays, which can lead to amorphous films, especially in case of multielement materials. Nevertheless, the greatest deviations of the film composition from the stoichiometry of the target occur in the transition regime: films obtained in this condition show a selective deficiency in the lighter elements due to the preferential scattering by the gas buffer (see above) [2–4]. This issue can be mitigated by using an O₂ gas buffer for the deposition of oxides: in this way it is possible to compensate the formation of oxygen vacancies within the film [18,22]. In the case of LLZTO the use of molecular oxygen as a background gas during the PLD manufacture can minimize oxygen losses but cannot compensate for the lithium losses. Therefore, for LLZTO thin film manufacture by PLD, as well as for all lithium-containing oxides, the diffusion regime is to be preferred. In fact, at pressures higher than 1 Pa the background gas confines the plasma and slows down its expansion, thus resulting in atomic/cluster species moving slowly with similar velocities. In this case, even in the presence of complex stoichiometry, the target composition is better preserved. Owing to this here we compare the manufacture of LLZTO PLD films carried out at 10^{-3} Pa (vacuum regime) and at 10 Pa of O₂ (diffusion regime).

TEM micrographs of nanoparticles deposited from the plume over TEM grids are shown in the Figure 1 to evaluate the impact of the background pressure on the morphology of mass deposits on the film substrate at the beginning of the PLD deposition.

In both conditions the presence of spherical particles superimposed to a dense background suggest that the films growth process can be described by a gas-phase condensation and coalescence of droplets. Most of the particles are smaller than 20 nm for both deposition conditions, suggesting that condensation from plasma is the prevailing process in particles formation. More in details in both pressure conditions a wide distribution of particle sizes can be observed: apparently the majority of nanoparticles shows sizes in the 10–20 nm range, forming the background layer, whereas a non-negligible fraction of larger particles with diameters in the hundreds of nanometres range is also present. Larger particles are likely emitted directly from the target as molten droplets [20], as can be observed in the Figure 1b inset. On the contrary, smaller particles likely derive from the condensation of the gaseous component from the plasma and their nucleation and growth is facilitated by the presence of the gas buffer in the ablation process [21]. The effect of confinement of the gas buffer, on the other hand, reduce the possibility that larger particles arrive on the substrate

surface [20]. These effects matches the differences observed in the particle size distributions reported in Figure 1c,f for coatings deposited at pressure of 10^{-3} Pa and 10 Pa, respectively.

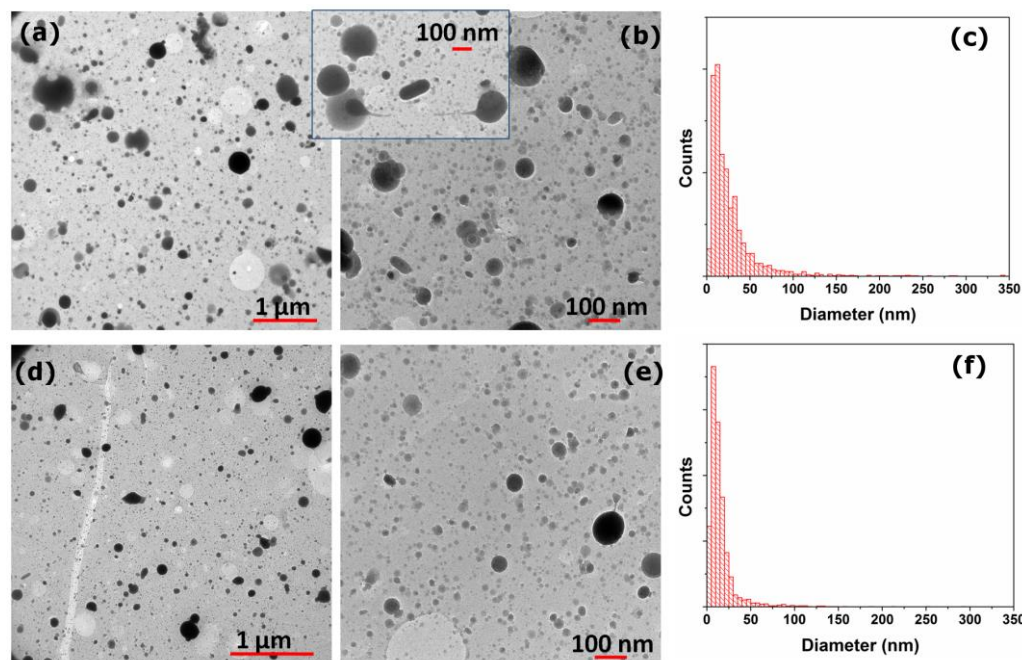


Figure 1. TEM images registered on LLZTO film deposited for 10 min (a,b) in vacuum (10^{-3} Pa) and (d,e) at 10 Pa of O_2 gas buffer. Particles size distribution obtained from different TEM images of film deposited (c) at 10^{-3} Pa and (f) at 10 Pa of O_2 .

A mean diameter of 27 nm is observed for particles deposited at 10^{-3} Pa, while those deposited at 10 Pa of O_2 show a much smaller mean diameter of about 16 nm. This evidence suggests that even in the first stages of film growth the presence of the background gas has a remarkable impact on the LLZTO film properties.

Larger differences in the film morphologies are more evident after 3 h of deposition in the different background atmosphere as highlighted in the SEM micrographs shown in the Figure 2.

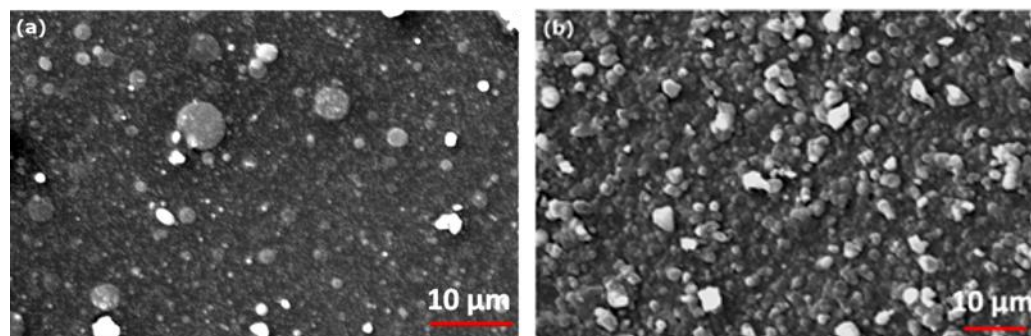


Figure 2. SEM images registered on LLZTO deposited film (a) at 10^{-3} Pa and (b) at 10 Pa of O_2 gas buffer.

Films deposited at 10^{-3} Pa (Figure 2a) shows the presence of round shaped micro-particles randomly distributed on a uniform and compact layer of smaller particles. On the contrary the film deposited O_2 , is characterized by a closely packed arrangement of nano- and micro- particles superimposed on a structured and compact background. The edge shape of the particles suggests the presence of crystalline domains.

The XRD patterns of the LLZTO target and of films deposited at different pressures, are shown in the Figure 3. All the peaks in the spectrum of the target can be assigned to cubic LLZTO phase [JCPDS 45-109].

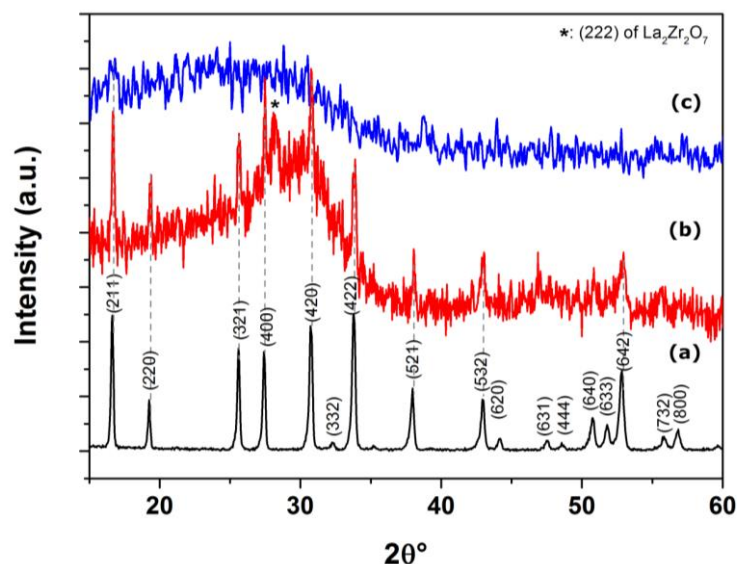


Figure 3. XRD patterns of LLZTO (a) target material, film deposited (b) at 10 Pa of O₂ gas buffer and (c) at 10^{−3} Pa.

The XRD pattern of the film deposited in vacuum (10^{−3} Pa) is characterized by a featureless broad undulation of the background thus proving the amorphous nature of the deposits. Otherwise, the XRD pattern of the film deposited at pressure of 10 Pa of O₂ shows few sharp peaks assignable to LLZTO. Moreover, the spurious peak at 28.4 2θ°, can possibly be assigned to La₂Zr₂O₇ (LZO) [PDF 01-071-2363], thus suggesting a lithium depletion during the deposition. No contribution from the steel substrate can be observed in XRD patterns of the deposited films.

In summary, the PLD of LLZTO in vacuum lead to the formation of amorphous films, while deposition under diffusion regime conditions allowed the manufacture of films with a certain degree of crystallinity. This is because, by depositing with a background gas pressure of 10 Pa, the species present in the plasma are kinetically slowed down, resulting in similar arrival times on the substrate surface. As a result, it becomes possible to preserve, at least partially, the stoichiometry and crystallinity of the target material. Nevertheless, the consistent difference in mass between lithium and the other ablated species led to an unavoidable Li-loss during the expansion of the plasma plume.

3.2. PLD Films from Li₂O-Enriched LLZTO Targets

The experimental evidence of the lithium depletion from the target stoichiometry suggests the need of an enrichment by Li₂O of the LLZTO target. Thus PLD in vacuum and in the diffusion regime was replicated on the new target material. XRD and Raman spectra, acquired on both the films and the target material, are shown in Figure 4.

Due to the very poor scattering factor of Li₂O, no additional peak is detected in the pristine target spectrum constituted by a 6% Li₂O enriched LLZTO pellet. On the contrary the XRD pattern of the deposited film at 10 Pa of O₂ do not show evidence of LZO segregation thus suggesting a successful compensation of the lithium loss suffered during the PLD deposition. Unfortunately, no clues can be inferred from the XRD pattern of the film grown under vacuum due to its homogeneous amorphous nature.

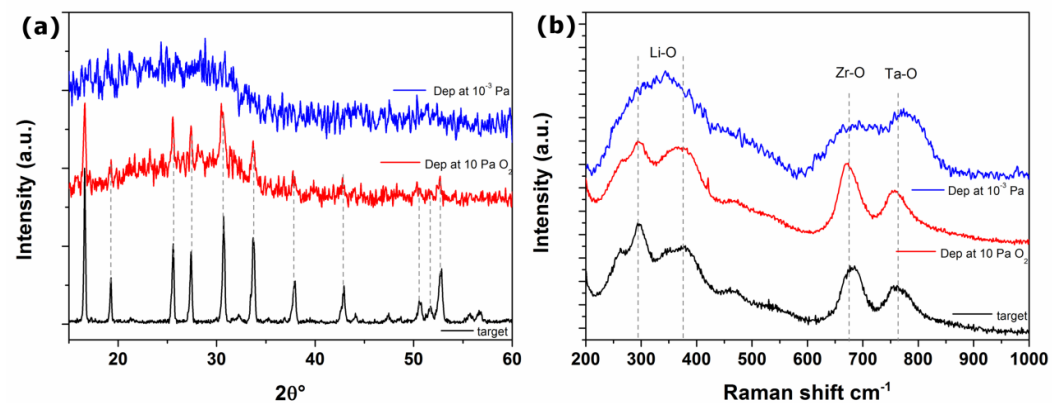


Figure 4. (a) XRD patterns and (b) Raman spectrum of LLZTO target material, film deposited at 10 Pa of O_2 gas buffer and in vacuum.

Raman spectroscopy allows to obtain information about the eventual short-range structural order of the deposited films. In agreement with XRD results, the Raman spectrum of the target material (Figure 4b) shows the vibrational fingerprint of cubic garnet phase of LLZTO [23–26]. In particular, all bands in the region $< 300\text{ cm}^{-1}$ are related to LiO_6 octahedral unit, while in the region $300\text{--}500\text{ cm}^{-1}$ are attributable to vibrational bending of LiO_4 tetrahedral unit. Bands centered at 670 and 760 cm^{-1} can be assigned to the stretching modes of ZrO_6 and TaO_6 octahedra, respectively. Unfortunately, modes related to the vibrations of the La-O bonds are not observable, since related peaks fall in the below 150 cm^{-1} [25,27], beyond our experimental capabilities.

Apparently, Raman spectra of the film deposited at 10 Pa of O_2 retain all target spectral features, in terms of either peaks position or shape. On the contrary broad bands, centred in the same spectral region of the main signals of LLZTO, are visible in the spectrum of films deposited at 10^{-3} Pa. These vibrational features likely originate from the LLZTO-based amorphous phase, since in disordered system in phase atomic vibrations are impeded.

In summary also in this case, the deposited films are different from both morphological and chemical point of view depending on the deposition conditions. Such differences originate from the impact of the deposition atmosphere on the plasma, its expansion and condensation.

3.3. Impact of the Post-PLD Annealing

In the attempt to restore the crystalline structure and to densify the films, the deposits have been annealed at high temperature. Song et al. [28] suggest that annealing at $600\text{ }^\circ\text{C}$ can be appropriate for LLZO films to improve their crystallinity, density and uniformity wither from a chemical or morphological point of view, while heat treatment at lower temperatures (500 and $550\text{ }^\circ\text{C}$) fail. Despite this Saccoccio et al. [15], observed, in PLD films post annealed in air at $600\text{ }^\circ\text{C}$, the formation of a crystalline LZO phase with a detrimental impact on the ionic conductivity. The LZO impurity is common and difficult to eliminate, even after the LLZTO enrichment with additional lithium, due to the evaporation of lithium from thin films with a high surface-to-volume ratio [19]. To mitigate this problem, one approach is to process the film at lower annealing temperature and/or reduce the duration of heat treatments. Since annealing at lower temperature does not improve the crystallization of cubic LLZTO here we study the impact of a sharp post-PLD thermal annealing at $600\text{ }^\circ\text{C}$ for only 5 min.

The XRD, SEM, and Raman characterizations of films collected after the post-PLD thermal annealing in air and in pure oxygen flow are shown in the Figure 5.

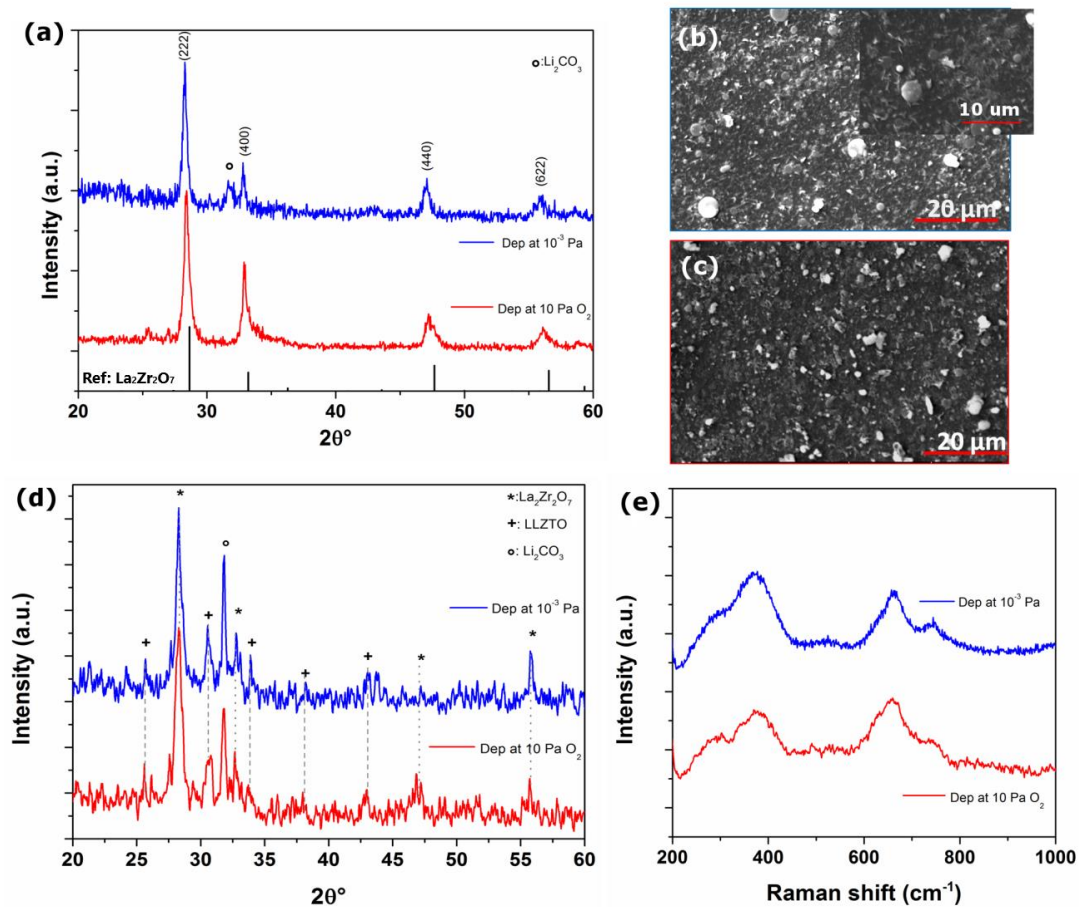


Figure 5. (a) XRD patterns of LLZTO film deposited at 10 Pa of O_2 gas buffer and in vacuum and annealed in air; SEM images of film deposited (b) in vacuum and (c) at 10 Pa of O_2 annealed in air, (d) XRD patterns and (e) Raman spectra of LLZTO film deposited at 10 Pa of O_2 gas buffer and in vacuum and annealed in O_2 flow.

Unfortunately, after heat treatments in air a deterioration in the film quality was observed, both morphologically and chemically. XRD patterns show the presence of a single crystalline phase likely attributed to LZO [PDF 01-071-2363] (see Figure 5a) in both films prepared in vacuum or at 10 Pa of O_2 . Moreover Raman spectra for these samples (not shown) shows the presence of a broad peak, not clearly distinguishable from the substrate signal, at $\sim 300\text{ cm}^{-1}$ also due to LZO [29].

The formation of LZO is a direct clue of the extended loss of lithium from the garnet lattice: being the annealing temperature only partially compatible with direct losses via the formation of gaseous Li-containing molecules [15], the lithium loss may also occur via the formation of lithium carbonate over the surface of the pristine LLZTO particles. Generally speaking, LLZO is highly reactive towards moisture and CO_2 under air exposure at moderate temperatures: previous studies reported that it can easily react with air humidity and CO_2 to form a thin Li_2CO_3 layer on the surface [30–33].

Turning to the analysis of the film morphologies after the thermal annealing, the SEM micrographs, shown in Figure 5b,c, highlights a sharp change in morphology for both the films after the annealing (see Figure 2 for a direct comparison): needle-shaped structures are present on a uniform background. One may speculate that the obtained films are less dense due to lithium loss, resulting in the formation of needle-like structures composed of LZO nanograins.

Since annealing treatments in O_2 atmosphere has been demonstrate to have a beneficial effect on the crystallinity of thin films of oxides [34] and with the aim to mitigate Li-loss and the detrimental formation of Li_2CO_3 , we annealed the films in oxygen flow using the

same thermal treatment as in air atmosphere. As can be observed from the XRD images in Figure 5d, these treatments lead to the formation of mixed partially crystalline LLZTO and LZO for both the film. Therefore, also in the case of annealings carried out in pure oxygen flows, lithium loss occurs, likely via the gas-phase, thus leading to the partial crystallization of the LZO phase.

The Raman spectra (shown in Figure 5e) exhibit signals likely attributed to LLZTO vibrational modes. Comparing the Raman spectra of the film deposited at 10 Pa of O₂ before (see Figure 4b for a direct comparison) and after annealing, a broadening of the Raman signals is observed after annealing, confirming the deterioration of the film crystalline structure.

3.4. Towards a Crystalline and Compact LLZTO Film via PLD

Overall, the manufacture of LLZTO films from Li₂O-enriched LLZTO deposited in oxygen atmosphere is the best compromise to obtain a crystalline LLZTO films. This confirms that a gas pressure within the diffusion regime helps to retain target composition and crystallinity in the deposited film, especially for oxides with complex stoichiometry like ZZTO. To shed more light on the film homogeneity across the surface and the cross section we further analysed this material using FIB-SEM. In Figure 6 SEM images and EDS elemental mapping of film deposited at 10 Pa of O₂ are shown. In particular, Figure 6a is acquired on film surface, while Figure 6b is a cross-section view.

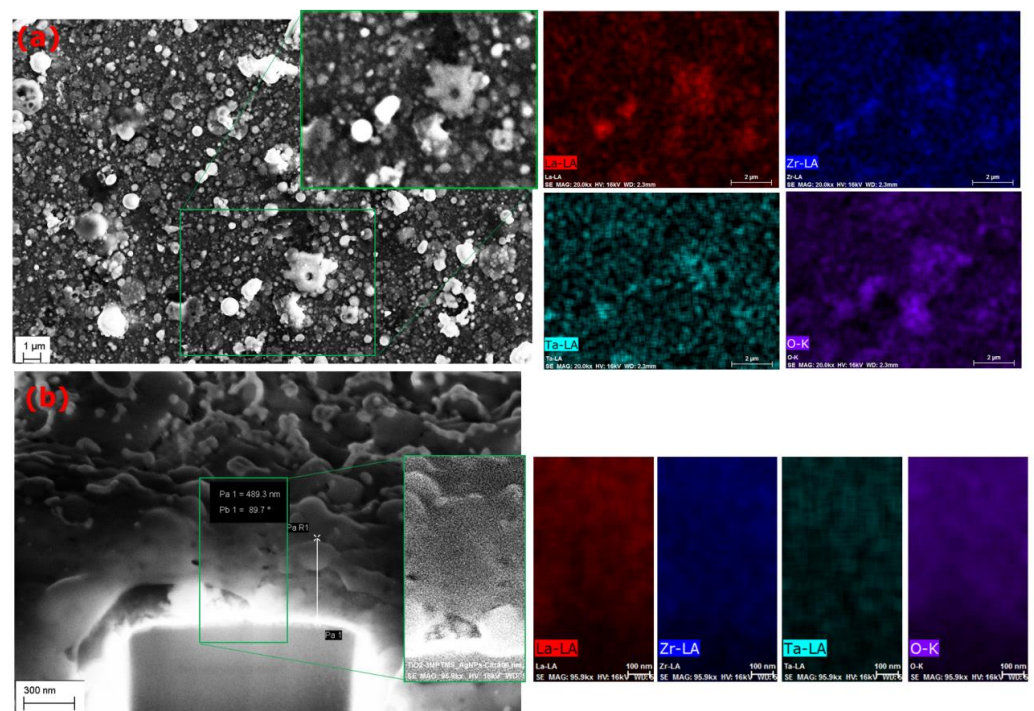


Figure 6. SEM image of LLZTO film deposited at 10 Pa Of O₂ (a) and its cross-section obtained by FIB (b) with EDS elemental mapping of La (red), Zr (blue), Ta (cyan), and O (purple) within the area reported in the inset.

From the cross-section image, it is possible to observe that the film is composed of a dense background layer with a thickness of hundreds of nanometers, onto which particles of varying sizes ranging from tens of nanometers to microns are superimposed. EDS mapping images demonstrate the homogeneous distribution of La, Zr, Ta, and O at the nanoscale both on the surface and throughout the thickness of the film.

4. Conclusions

LLZTO thin films were deposited using the PLD technique. To investigate the influence of the deposition atmosphere on the film's properties, PLD was performed in vacuum (10^{-3} Pa) and at 10 Pa of O₂ gas buffer. Additionally, to address the issue of lithium losses, the starting material was enriched with a small percentage of lithium oxide.

The obtained films exhibit notable differences, both morphologically and chemically, as the deposition atmosphere affects the dynamics of the expanding plasma generated by laser ablation. Vacuum deposition leads to the formation of amorphous films, while depositing within the pressure range of the diffusion regime yields crystalline films.

Upon thermal treatment at 600 °C, a partial lithium loss was observed in the case of annealing conducted in an oxygen flow, whereas crystallization of the single-phase impurity (LZO) was observed for films annealed in air.

Taking into account the overall data, it is evident that to obtain thin films of complex oxides like LLZTO, it is advisable to deposit under oxygen pressure. This approach results in compact, crystalline films with a homogeneous elemental distribution on the surface and throughout the film's depth, closely resembling the composition of the target material.

In order to further enhance the quality of these films, other deposition parameters can be varied. Specifically, controlling the target-to-substrate distance will provide the means to fine-tune surface roughness, while regulating the substrate temperature will aid in achieving films with larger crystalline domains.

Author Contributions: Conceptualization, M.C., A.D.B., S.B. and R.T.; methodology, M.C., A.D.B. and R.T.; formal analysis, M.C., A.C. and A.D.B.; investigation, A.C., A.D.B., A.G., M.C. and S.B.; data curation, M.C., S.B., A.D.B. and R.T.; writing—original draft preparation, A.D.B. and M.C.; writing—review and editing, M.C., S.B. and A.D.B.; supervision, S.B., A.D.B. and R.T. All authors have read and agreed to the published version of the manuscript.

Funding: This research was funded "PO FESR Basilicata 2014-2020" (MOBAS 4.0—CUP: G49J19001340006) from Regione Basilicata. The contribution of S.B. and A.C. to this study was carried out within the NEST—Network for Energy Sustainable Transition and received funding from the European Union Next-GenerationEU (PIANO NAZIONALE DI RIPRESA E RESILIENZA (PNRR)—MISSIONE 4 COMPONENTE 2, INVESTIMENTO 1.3—D.D. 1561 11/10/2022, B53C22004070006). This manuscript reflects only the authors' views and opinions, neither the European Union nor the European Commission can be considered responsible for them. All Sapienza staff within the NEST project participate to this action under the frame of the grant PE2421852F05911E.

Institutional Review Board Statement: Not applicable.

Informed Consent Statement: Not applicable.

Data Availability Statement: Not applicable.

Conflicts of Interest: The authors declare no conflict of interest. The funders had no role in the design of the study; in the collection, analyses, or interpretation of data; in the writing of the manuscript; or in the decision to publish the results.

References

1. Schneider, C.W.; Lippert, T. Laser Ablation and Thin Film Deposition. In *Laser Processing of Materials: Fundamentals, Applications and Developments*; Schaaf, P., Ed.; Springer: Berlin/Heidelberg, Germany, 2010; pp. 89–112.
2. Shepelin, N.A.; Tehrani, Z.P.; Ohannessian, N.; Schneider, C.W.; Pergolesi, D.; Lippert, T. A Practical Guide to Pulsed Laser Deposition. *Chem. Soc. Rev.* **2023**, *52*, 2294–2321. [[CrossRef](#)] [[PubMed](#)]
3. Schneider, C.W.; Lippert, T. PLD Plasma Plume Analysis: A Summary of the PSI Contribution. *Appl. Phys. A Mater. Sci. Process.* **2023**, *129*, 138. [[CrossRef](#)]
4. Scharf, T.; Krebs, H.U. Influence of Inert Gas Pressure on Deposition Rate during Pulsed Laser Deposition. *Appl. Phys. A Mater. Sci. Process.* **2002**, *75*, 551–554. [[CrossRef](#)]
5. Fei, H.; Liu, Y.; Wei, C.; Zhang, Y.; Feng, J.; Chen, C.; Yu, H. Poly(propylene carbonate)-based Polymer Electrolyte with an Organic Cathode for Stable All-Solid-State Sodium Batteries. *Acta Phys.-Chim. Sin.* **2020**, *36*, 1905015. [[CrossRef](#)]
6. Singh, J.P.; Paidi, A.K.; Lee, S. Growth strategies of Li₇La₃Zr₂O₁₂ electrolytes for Li-ion thin film battery. *Chem. Eng. J. Adv.* **2023**, *16*, 100532. [[CrossRef](#)]

7. Adams, S.; Rao, R.P. Ion Transport and Phase Transition in $\text{Li}_{7-x}\text{La}_3(\text{Zr}_{2-x}\text{M}_x)\text{O}_{12}$ ($\text{M} = \text{Ta}^{5+}, \text{Nb}^{5+}, x = 0, 0.25$). *J. Mater. Chem.* **2012**, *22*, 1426–1434. [[CrossRef](#)]
8. Kim, Y.; Yoo, A.; Schmidt, R.; Sharafi, A.; Lee, H.; Wolfenstine, J.; Sakamoto, J. Electrochemical Stability of $\text{Li}_{6.5}\text{La}_3\text{Zr}_{1.5}\text{M}_{0.5}\text{O}_{12}$ ($\text{M} = \text{Nb}$ or Ta) against Metallic Lithium. *Front. Energy Res.* **2016**, *4*, 20. [[CrossRef](#)]
9. Shen, F.; Guo, W.; Zeng, D.; Sun, Z.; Gao, J.; Li, J.; Zhao, B.; He, B.; Han, X. A Simple and Highly Efficient Method toward High-Density Garnet-Type LLZTO Solid-State Electrolyte. *ACS Appl. Mater. Interfaces* **2020**, *12*, 30313–30319. [[CrossRef](#)]
10. Deng, T.; Ji, X.; Zhao, Y.; Cao, L.; Li, S.; Hwang, S.; Luo, C.; Wang, P.; Jia, H.; Fan, X.; et al. Tuning the Anode–Electrolyte Interface Chemistry for Garnet-Based Solid-State Li Metal Batteries. *Adv. Mater.* **2020**, *32*, 2000030. [[CrossRef](#)]
11. Yang, G.; Abraham, C.; Ma, Y.; Lee, M.; Helfrick, E.; Oh, D.; Lee, D. Advances in Materials Design for All-Solid-state Batteries: From Bulk to Thin Films. *Appl. Sci.* **2020**, *10*, 4727. [[CrossRef](#)]
12. Hoinkis, N.; Schuhmacher, J.; Leukel, S.; Loho, C.; Roters, A.; Richter, F.H.; Janek, J. Particle Size-Dependent Degradation Kinetics of Garnet-Type $\text{Li}_{6.5}\text{La}_3\text{Zr}_{1.5}\text{Ta}_{0.5}\text{O}_{12}$ Solid Electrolyte Powders in Ambient Air. *J. Phys. Chem.* **2023**, *127*, 8320–8331. [[CrossRef](#)]
13. Jeong, W.; Park, S.S.; Yun, J.; Shin, H.R.; Moon, J.; Lee, J.W. Tailoring grain boundary structures and chemistry of $\text{Li}_7\text{La}_3\text{Zr}_2\text{O}_{12}$ solid electrolytes for enhanced air stability. *Energy Storage Mater.* **2023**, *54*, 543–552. [[CrossRef](#)]
14. Ma, Z.; Zhao, B.; Li, W.; Jiao, S.; Gong, W.; Qiu, H.; Song, H.; Yu, M. Effects of fabrication atmosphere conditions on the physico-chemical properties of garnet electrolyte. *Ionics* **2022**, *28*, 2673–2683. [[CrossRef](#)]
15. Saccoccio, M.; Yu, J.; Lu, Z.; Kwok, S.C.T.; Wang, J.; Yeung, K.K.; Yuen, M.M.F.; Ciucci, F. Low Temperature Pulsed Laser Deposition of Garnet $\text{Li}_{6.4}\text{La}_3\text{Zr}_{1.4}\text{Ta}_{0.6}\text{O}_{12}$ Films as All Solid-State Lithium Battery Electrolytes. *J. Power Sources* **2017**, *365*, 43–52. [[CrossRef](#)]
16. Indrizzi, L.; Ohannessian, N.; Pergolesi, D.; Lippert, T.; Gilardi, E. Pulsed Laser Deposition as a Tool for the Development of All Solid-State Microbatteries. *Helv. Chim. Acta* **2021**, *104*, e2000203. [[CrossRef](#)]
17. Curcio, M.; De Bonis, A.; Brutti, S.; Santagata, A.; Teghil, R. Pulsed Laser Deposition of Thin Films of TiO_2 for Li-Ion Batteries. *Appl. Surf. Sci. Adv.* **2021**, *4*, 100090. [[CrossRef](#)]
18. Smaldone, A.; Brutti, S.; De Bonis, A.; Ciarfaglia, N.; Santagata, A.; Teghil, R. Iron Doped LiCoPO_4 Thin Films for Lithium-Ion Microbatteries Obtained by Pulsed Laser Deposition. *Appl. Surf. Sci.* **2018**, *445*, 56–64. [[CrossRef](#)]
19. Park, J.S.; Cheng, L.; Zorba, V.; Mehta, A.; Cabana, J.; Chen, G.; Doeff, M.M.; Richardson, T.J.; Park, J.H.; Son, J.W.; et al. Effects of Crystallinity and Impurities on the Electrical Conductivity of Li-La-Zr-O Thin Films. *Thin Solid Films* **2015**, *576*, 55–60. [[CrossRef](#)]
20. Amoruso, S.; Toftmann, B.; Schou, J. Thermalization of a UV Laser Ablation Plume in a Background Gas: From a Directed to a Diffusionlike Flow. *Phys. Rev. E* **2004**, *69*, 056403. [[CrossRef](#)] [[PubMed](#)]
21. Ojeda-G-P, A.; Döbeli, M.; Lippert, T. Influence of Plume Properties on Thin Film Composition in Pulsed Laser Deposition. *Adv. Mater. Interfaces* **2018**, *5*, 1701062. [[CrossRef](#)]
22. Hasabeldaim, E.; Ntwaeaborwa, O.M.; Kroon, R.E.; Motaung, D.E.; Coetsee, E.; Swart, H.C. Effect of PLD Growth Atmosphere on the Physical Properties of ZnO:Zn Thin Films. *Opt. Mater.* **2017**, *74*, 76–85. [[CrossRef](#)]
23. Tietz, F.; Wegener, T.; Gerhards, M.T.; Giarola, M.; Mariotto, G. Synthesis and Raman Micro-Spectroscopy Investigation of $\text{Li}_7\text{La}_3\text{Zr}_2\text{O}_{12}$. *Solid State Ion.* **2013**, *230*, 77–82. [[CrossRef](#)]
24. Larraz, G.; Orera, A.; Sanjuán, M.L. Cubic Phases of Garnet-Type $\text{Li}_7\text{La}_3\text{Zr}_2\text{O}_{12}$: The Role of Hydration. *J. Mater. Chem. A* **2013**, *1*, 11419–11428. [[CrossRef](#)]
25. Pervez, S.A.; Kim, G.; Vinayan, B.P.; Cambaz, M.A.; Kuenzel, M.; Hekmatfar, M.; Fichtner, M.; Passerini, S. Overcoming the Interfacial Limitations Imposed by the Solid–Solid Interface in Solid-State Batteries Using Ionic Liquid-Based Interlayers. *Small* **2020**, *16*, 2000279. [[CrossRef](#)] [[PubMed](#)]
26. Ramos, E.; Browar, A.; Roehling, J.; Ye, J. CO_2 Laser Sintering of Garnet-Type Solid-State Electrolytes. *ACS Energy Lett.* **2022**, *7*, 3392–3400. [[CrossRef](#)]
27. Dhivya, L.; Karthik, K.; Ramakumar, S.; Murugan, R. Facile Synthesis of High Lithium Ion Conductive Cubic Phase Lithium Garnets for Electrochemical Energy Storage Devices. *RSC Adv.* **2015**, *5*, 96042–96051. [[CrossRef](#)]
28. Huang, X.; Lu, Y.; Song, Z.; Rui, K.; Wang, Q.; Xiu, T.; Badding, M.E.; Wen, Z. Manipulating Li_2O Atmosphere for Sintering Dense $\text{Li}_7\text{La}_3\text{Zr}_2\text{O}_{12}$ Solid Electrolyte. *Energy Storage Mater.* **2019**, *22*, 207–217. [[CrossRef](#)]
29. Garbayo, I.; Struzik, M.; Bowman, W.J.; Pfenninger, R.; Stilp, E.; Rupp, J.L.M. Glass-Type Polyamorphism in Li-Garnet Thin Film Solid State Battery Conductors. *Adv. Energy Mater.* **2018**, *8*, 1702265. [[CrossRef](#)]
30. Cheng, L.; Crumlin, E.J.; Chen, W.; Qiao, R.; Hou, H.; Franz Lux, S.; Zorba, V.; Russo, R.; Kostecki, R.; Liu, Z.; et al. The Origin of High Electrolyte-Electrode Interfacial Resistances in Lithium Cells Containing Garnet Type Solid Electrolytes. *Phys. Chem. Chem. Phys.* **2014**, *16*, 18294–18300. [[CrossRef](#)]
31. Sharafi, A.; Yu, S.; Naguib, M.; Lee, M.; Ma, C.; Meyer, H.M.; Nanda, J.; Chi, M.; Siegel, D.J.; Sakamoto, J. Impact of Air Exposure and Surface Chemistry on Li- $\text{Li}_7\text{La}_3\text{Zr}_2\text{O}_{12}$ Interfacial Resistance. *J. Mater. Chem. A* **2017**, *5*, 13475–13487. [[CrossRef](#)]
32. Chen, L.; Su, Y.; Zhang, J.; Zhang, H.; Fan, B.; Shao, G.; Zhong, M.; Wang, C.A. Nanosecond Laser Cleaning Method to Reduce the Surface Inert Layer and Activate the Garnet Electrolyte for a Solid-State Li Metal Battery. *ACS Appl. Mater. Interfaces* **2021**, *13*, 37082–37090. [[CrossRef](#)] [[PubMed](#)]

33. Xia, W.; Xu, B.; Duan, H.; Tang, X.; Guo, Y.; Kang, H.; Li, H.; Liu, H. Reaction Mechanisms of Lithium Garnet Pellets in Ambient Air: The Effect of Humidity and CO₂. *J. Am. Ceram. Soc.* **2017**, *100*, 2832–2839. [[CrossRef](#)]
34. Lotkov, E.S.; Baburin, A.S.; Ryzhikov, I.A.; Sorokina, O.S.; Ivanov, A.I.; Zverev, A.V.; Ryzhkov, V.V.; Bykov, I.V.; Baryshev, A.V.; Panfilov, Y.V.; et al. ITO film stack engineering for low-loss silicon optical modulators. *Sci. Rep.* **2022**, *12*, 6321. [[CrossRef](#)] [[PubMed](#)]

Disclaimer/Publisher's Note: The statements, opinions and data contained in all publications are solely those of the individual author(s) and contributor(s) and not of MDPI and/or the editor(s). MDPI and/or the editor(s) disclaim responsibility for any injury to people or property resulting from any ideas, methods, instructions or products referred to in the content.